

## Design of Ultra-Wideband MIMO Antenna with Dual Band Elimination Characteristics and Low Mutual Coupling

Ravindra Bakale<sup>1</sup>, Anil Nandgaonkar<sup>1</sup>, Shankar Deosarkar<sup>1</sup>, and Mahesh Munde<sup>2, \*</sup>

**Abstract**—The paper proposes the design of an ultra-wideband MIMO antenna with low mutual coupling and dual-band elimination characteristics. The proposed structure consists of a microstrip-fed monopole antenna with a stub to enhance the isolation for ultra-wideband applications. The dual rejection bands corresponding to WiMAX and WLAN frequencies are designed using electromagnetic band-gap structures of mushroom-type and placed close to the microstrip transmission line of the designed antenna. The isolation enhancement of  $|S_{21}| > 20$  dB is achieved over the impedance bandwidth by adding two counter-facing F-pattern stubs to the ground. The impedance bandwidth of 9 GHz (2.65–11.65 GHz) for VSWR  $< 2.13$  with the notch bands of 3.6–4.2 GHz and 5.15–5.87 GHz is obtained. The diversity gain, correlation coefficient, radiation pattern, TARC, and peak gain are also studied in the paper. The simulated and measured results are in close agreement with each other. Therefore, the proposed structure is a potential candidate for wireless communication.

### 1. INTRODUCTION

An unlicensed spectrum of 3.1–10.6 GHz is released for ultra-wideband (UWB) short-range wireless communication. The UWB multiple-input multiple-out (MIMO) systems are designed for wireless communications spectrum such as 3.3–3.8 GHz (WiMAX), INSAT operating between 4.5 and 4.8 GHz, WLAN (5.2–5.8 GHz) system, and 7.1–7.9 GHz (X band) which causes electromagnetic (EM) interference. So, MIMO antennas with band-notches are designed for UWB applications. The MIMO antennas are designed to satisfy the huge data rate requirements without additional transmitted power and frequency spectrum in the crowded scattering areas with different decoupling techniques to improve the isolation and polarization matching while minimizing the channel noise and multipath fading [1, 2]. The compact antenna design is achieved using an Asymmetric Coplanar Strip (ACS)-fed technique, and open stubs are integrated into the patches to obtain the band rejection at 4.9–6 GHz. An H-pattern slot is added to the ground to lower the mutual coupling  $< -20$  dB over 2.9–11.8 GHz. The MIMO antenna is designed using two square monopole antennas with a slotted ground to generate the isolation of more than 30 dB. U- and L-structured slots are used to achieve a band elimination at 3.3–3.8 GHz frequency over  $S_{11}$  bandwidth of 2.2–10.8 GHz [3, 4]. In [5, 6], a MIMO antenna with a dual-notch band is designed by arranging two circular patches in an orthogonal manner with two L-pattern slots embedded in it. Dual U-shaped branches are loaded to the ground to enhance the isolation  $> 20$  dB over impedance bandwidth (BW) of 2.68–12.50 GHz. A miniaturized MIMO antenna with a dual-notch band is designed for UWB application using a radiating patch and high isolation using a T-shaped stub in the ground. Dual bands are eliminated corresponding to WiMAX and WLAN by cutting dual elliptical slots on the patch with a useable BW of 2.6–20 GHz. A compact single band-notched at WLAN (5.725–5.825 GHz)

---

Received 22 June 2022, Accepted 16 August 2022, Scheduled 5 September 2022

\* Corresponding author: Mahesh Munde (mmunde@xaviertech.com).

<sup>1</sup> Dr. Babasaheb Ambedkar Technological University, Lonere 402103, India. <sup>2</sup> Department of Electronics and Telecommunication Engineering, St. Xavier's Technical Institute, Mumbai 400016, India.

UWB MIMO antenna with two symmetrical radiators on a substrate is designed over a 10 dB bandwidth of 3.1–11 GHz except for the notched band.

An H-pattern slot and a vertical stub are loaded to the ground to maximize the isolation  $> 18$  dB over the useful working bandwidth. A small-size single band rejection characteristics MIMO antenna is designed for UWB application. A microstrip transmission line fed rectangular slot acts as the main radiator while the WLAN band (5.15–5.85 GHz) is rejected using a z-shaped slot.

An inverted T-shaped slot and a vertical slot in a rectangular pattern are embedded in the ground to increase the isolation  $> 24.5$  dB over the band of 3.1–10.6 GHz [7, 8]. A novel dual-band notch Vivaldi MIMO antenna was designed for UWB application. WLAN and X band are notched at 5.3–5.8 GHz and 7.85–8.55 GHz using two different split-ring resonators (SRRs). A T-pattern slot is added to the ground so that isolation  $> 16$  dB is achieved over the impedance bandwidth of 2.9–11.6 GHz except for the notch bands. A tapered microstrip-fed UWB MIMO antenna with dual-band elimination characteristics is designed for wireless applications. Inverted L-pattern slits are loaded to the radiating elements to generate notch bands at IEEE INSAT and WLAN. The isolation enhancement of  $> 22$  dB is obtained over the working band of 2.93–20 GHz [9, 10]. A miniaturized triple-notch band UWB MIMO antenna is designed using two C-shaped slots embedded into each radiating element. The three notched bands at 3.4–3.9 GHz, 5.05–5.85 GHz, and 7.9–8.4 GHz are developed. A T-pattern stub is loaded to the ground to increase the isolation  $> 18$  dB over the 3.1–10.6 GHz frequency. A complementary splitting resonator (CSR) of hexagonal shape is added to the radiator to develop a two-notch band at 3.5 GHz and 5.5 GHz. The mutual coupling  $< -18$  dB is obtained over the useful operating band of 3–16 GHz [11, 12]. A small size MIMO antenna with dual-band elimination characteristics was designed for UWB application by adding an elliptical CSR to the monopole radiator to notch two bands at 3.5 GHz and 5.5 GHz, corresponding to WiMAX and WLAN, respectively. Slotted edge substrate technique was used to reduce inter-element coupling  $< -22$  dB over 3 to 13.5 GHz frequency band. A novel dual-notch band MIMO antenna was designed based on the Quasi Self Complementary technique for UWB application. A C-pattern slot is embedded in the radiator to eliminate the 5.8 GHz WLAN band, and a square ring is etched on the ground to reject WiMAX at 3.6 GHz with isolation  $> 20$  dB over the useful wideband from 2.4 to 12 GHz [13, 14]. A C-pattern slot and an unsymmetrical H-pattern slot are integrated with the patch to develop dual-band rejection at 5.5 GHz and 7.5 GHz. A stub is added to each defected ground structure so that mutual coupling  $< -22$  dB over the entire working band 2–16.8 GHz is achieved. A metamaterial-based MIMO antenna was designed for UWB application with circular polarization and high isolation. CSRRs are added to defected ground structure (DGS) so that the isolation  $> 15$  dB over the 2.5–10.6 GHz [15, 16]. In [17, 18], a miniaturized MIMO antenna was designed with useful bandwidth from 2.1–12 GHz. A split ring resonator (SRR) and elliptical slots are loaded to the ground to enhance the isolation  $> 20$  dB. A MIMO antenna is integrated with L-type parasitic branches and a fence-type structure to lower the mutual coupling  $< -25$  dB in the working bandwidth of 3.1–11 GHz. A thin stub is loaded in the ground to notch the WLAN band from 4.9–6.4 GHz in a four-element UWB MIMO antenna operating in 2–12 GHz with isolation  $> 17$  dB [19]. A Minkowski fractal is grounded, and the parasitic stub is arranged at  $45^\circ$  between the radiating elements so that isolation is  $> 17$  dB throughout the entire wideband of 3.1–12 GHz. A small size E-pattern slot is cut on both the patches to achieve a band-notch at 5.15–5.85 GHz [20]. A dual-polarized microstrip-fed MIMO antenna designed for UWB wireless application with an impedance BW of 3.1–10.6 GHz. Dual bands are notched at 5 GHz and 8 GHz corresponding to WLAN and X bands by integrating an open-ended slot and a SRR with the ground. A Y-pattern defected structure is added to the ground so that the isolation is  $> 15$  dB [21]. In [22], A MIMO antenna with CPW-feed was designed for UWB applications with dual-band elimination characteristics. The X band communication downlink band is notched by optimizing a SRR, and the WLAN band is rejected using the integration of a protruded stub and arc-shaped strips. The mutual coupling is less than  $-15$  dB using the protruded stub over an impedance BW of 3.4–12 GHz. A coplanar waveguide fed MIMO antenna is optimized for the UWB application with dual-band elimination characteristics and high isolation. Annular slots and rectangular slots are embedded in the radiator to reject two bands at WLAN and WiMAX. Y-shaped branches are etched between antenna elements so that the isolation is  $> 21$  dB over an impedance BW of 2.36–12 GHz [23]. A MIMO antenna with CPW-feed was designed with dual-band rejection characteristics and high isolation over working bandwidth of 3–16 GHz. A cup-pattern branch is loaded to the ground

to generate a WLAN notch from 4.94–5.85 GHz, and a step impedance resonator is embedded with a microstrip line to notch the X band from 7.24–7.85 GHz. Periodic strip branches are printed on the ground so that isolation  $|S_{21}| > 20$  dB [24]. In [25], a miniaturized four-element triple-notch band UWB MIMO antenna was designed by adding slits and slots on the radiating elements, decoupling structure, and defected ground structure, respectively. The triple notch bands are achieved at 3.5 GHz, 5.5 GHz, and 7.5 GHz center frequencies corresponding to WiMAX, WLAN, and X bands, respectively.

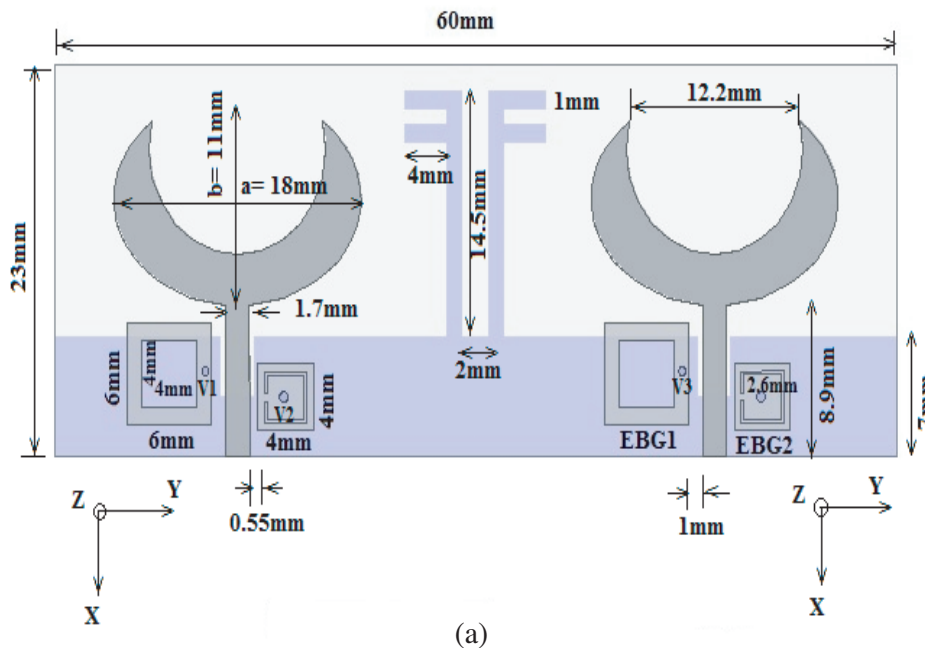
A UWB MIMO antenna with low inter-element coupling and dual-band elimination characteristics is designed using monopole radiators over a 10 dB bandwidth of 2.65–11.65 GHz for VSWR  $< 2.13$ . The dual bands are notched at 3.6–4.2 GHz and 5.15–5.87 GHz representing WiMAX and WLAN using Electromagnetic Band-Gap (EBG) structures of mushroom type printed near the microstrip transmission feed line of the antenna. EBG structures act as a band-stop filter in the desired frequency band with high impedance and contain a shorting pin (Via) and metallic patch, which connects the patch to the ground [26, 27]. The two counter-faced F-pattern stubs are loaded to the ground so that isolation is  $> 15$  dB over the frequency range 2.65–11.65 GHz. This contribution by the authors is helpful in the design of the proposed structure.

The sequence of paper is planned as the proposed antenna design is explained in Section 2.  $S$  parameter studies such as  $S_{11}$ ,  $S_{21}$ , and surface current distribution are discussed in Section 3. Fabrication, testing, result analysis, and diversity performance are covered in Section 4, and Section 5 highlights the conclusion of the proposed antenna.

## 2. DESIGN OF THE PROPOSED ANTENNA

A microstrip-fed dual-notch band UWB MIMO antenna is designed on a substrate of size 23 mm  $\times$  60 mm  $\times$  1.53 mm with an FR4 material having dielectric permittivity 4.4 and loss tangent 0.027. The proposed structure is designed with a monopole radiator having an impedance bandwidth of 2.65–11.65 GHz (138%) except for the notched band of WiMAX and WLAN. Mushroom-type EBG design structures are mounted close to the transmission feed line to achieve the rejection of bands at 3.60–4.20 GHz and 5.15–5.87 GHz frequencies.

The two counter-faced F-pattern stubs are etched in the ground to maximize the isolation  $|S_{21}| > 15$  dB. The designed antenna with dimensions is depicted in Figure 1(a). Figures 1(b) and 1(c) represent the EBG structure and its equivalent circuit.



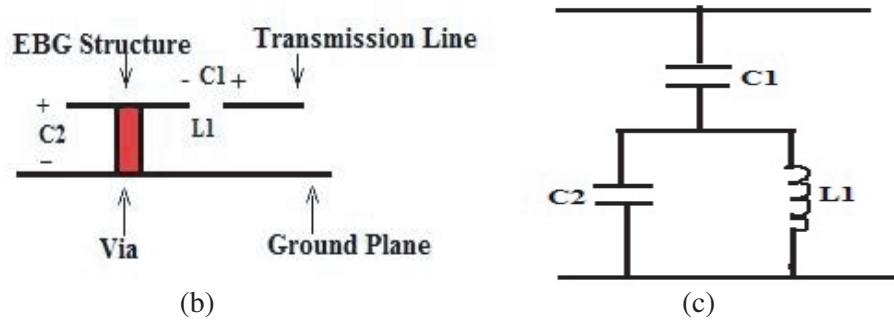


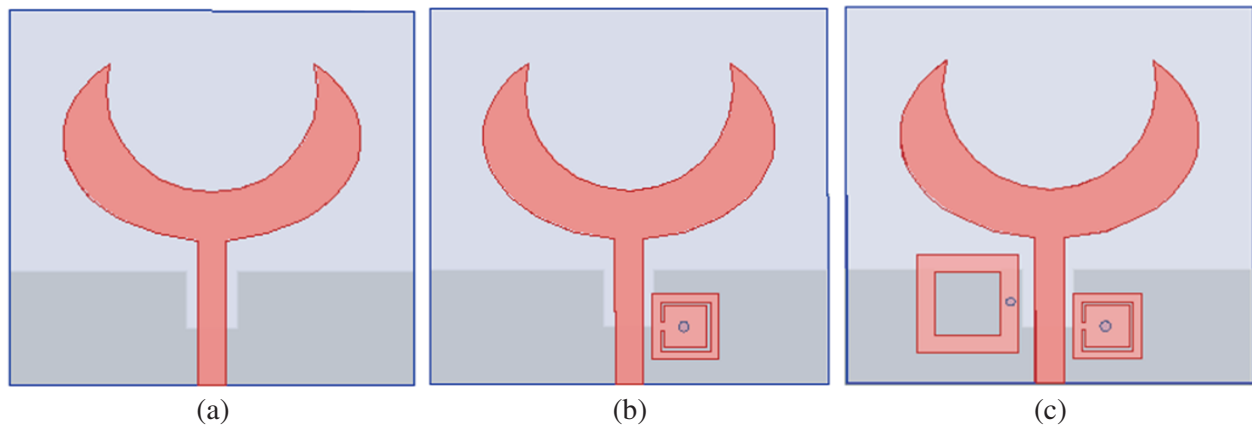
**Figure 1.** Proposed structure. (a) Design and dimensions. (b) EBG structure. (c) Equivalent of EBG.

### 3. ANALYSIS OF PROPOSED STRUCTURE

The design and development of the proposed structure are explained in the following subsections. The dimensions of both monopole antenna and ground are optimized in achieving the wideband operation of the antenna. The band notches are incorporated in the design using an EBG structure and placed close to the microstrip transmission feed line. The isolation is enhanced by  $> 15$  dB by loading two counter-faced F-shaped stubs to the ground. The proposed structure is simulated by ANSYS HFSS to analyze the performance in terms of  $S$  parameters.

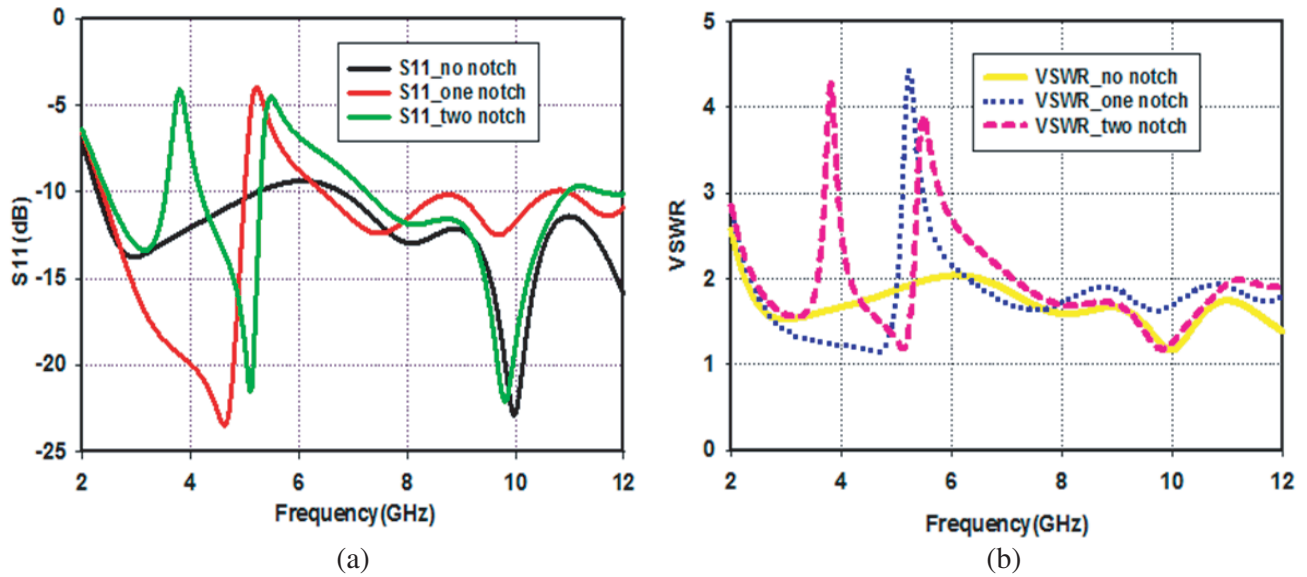
#### 3.1. Analysis of UWB Antenna with Notches and EBG Unit Cells

Figure 2(a) represents a microstrip-fed UWB monopole antenna. An electromagnetic bandgap type structure is loaded in the proposed structure to reject the WLAN band as mentioned in Figure 2(b). The WiMAX frequency band is rejected ( $S_{11} > -10$  dB) by loading another EBG structure as depicted in Figure 2(c). Simulated results such as  $S_{11}$  and VSWR are plotted in Figure 3(a) and Figure 3(b). The working bandwidth ( $S_{11} < -10$  dB) from 2.6–12 GHz is achieved except for the notched band of WIMAX from 3.6–4.2 GHz and WLAN of 5.2–5.87 GHz.



**Figure 2.** UWB antenna with notches. (a) UWB antenna. (b) Single notch-band. (c) Dual notch-band.

Figures 4(a) and 4(b) depict transmission line model for analysis of different EBG unit cells to validate the band gap characteristics. The model is simulated in an eigen-mode solution and dispersion diagram based on rectangular (irreducible) Brillouin zone. The band gap that exists in EBG1 and EBG2 structure are illustrated in Figures 4(c) and 4(d), respectively. The first band gap (light blue part) for EBG1 is between mode 1 and mode 2, centered at  $f_{c1} = 3.7$  GHz with lower cut-off frequency

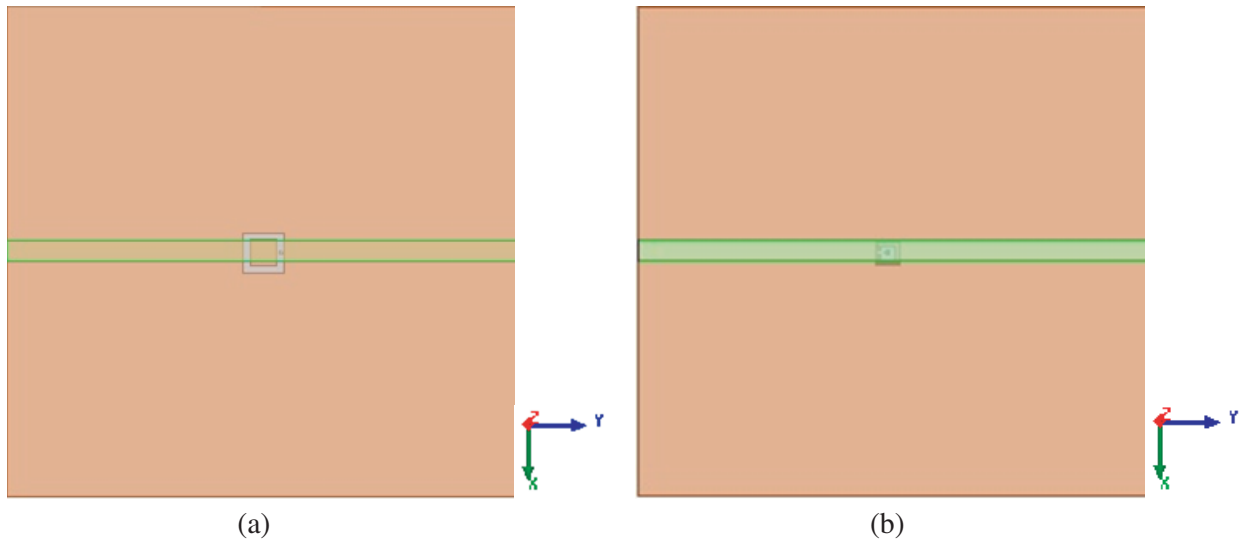


**Figure 3.** Simulation of UWB antenna with and without notches. (a)  $S_{11}$ . (b) VSWR.

$f_{l1} = 3.2$  GHz and higher cut-off frequency  $f_{h1} = 4.2$  GHz. The second band gap (green part) for EBG2 is between mode 1 and mode 2 centered at  $f_{c2} = 5.25$  GHz with a lower and higher cut-off frequencies of  $f_{l2} = 4.6$  GHz and  $f_{h2} = 5.9$  GHz, respectively.

### 3.2. Analysis of Ultra-Wideband MIMO Antenna with Notches

Microstrip-fed UWB monopole MIMO antenna with improved isolation using two counter-faced F-pattern stubs are shown in Figure 5(a). The EBG structure is positioned close to the microstrip feed line to eliminate the WLAN band ( $S_{11} > -10$  dB) as represented in Figure 5(b). In Figure 5(c), another EBG structure is added to the proposed structure to notch the WiMAX band. The  $S$  parameter results such as  $S_{11}$  and  $S_{21}$  are depicted in Figure 6(a) and Figure 6(b). A working bandwidth ( $S_{11} < -10$  dB) of 2.65–11.65 GHz except the notch bands for  $VSWR < 2.13$  is achieved. The rejected bands ( $S_{11} > -10$  dB) are 3.6–4.2 GHz and 5.15–5.87 GHz, corresponding to WiMAX and WLAN, respectively. The isolation between antenna elements ( $S_{21}$ )  $> 15$  dB over 6–8 GHz and greater than 20 dB in (2–6 GHz) as well as (8–12 GHz) frequency band, respectively.



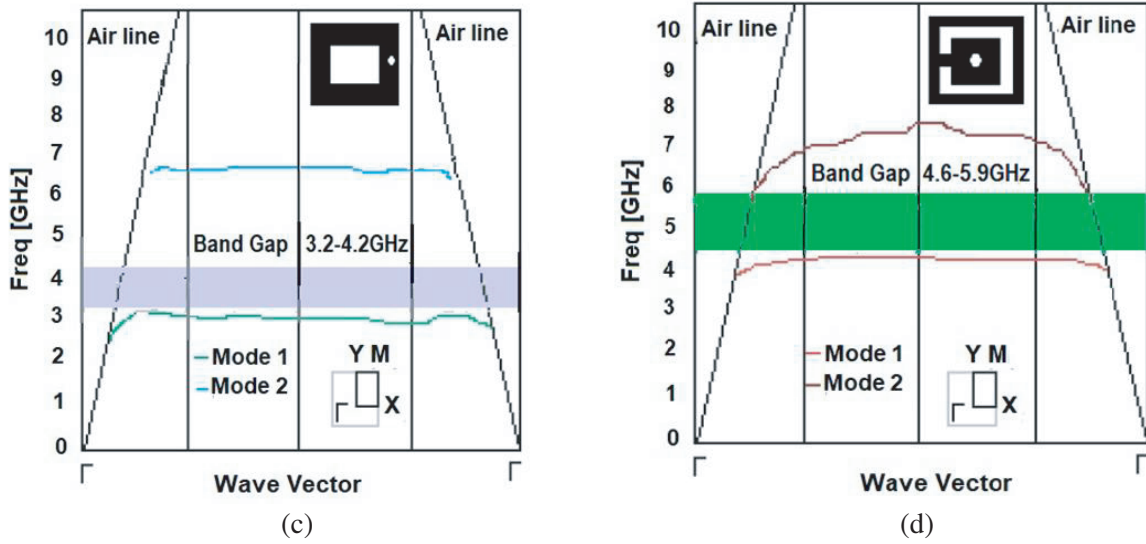


**Figure 4.** Analysis using transmission line technique. (a) EBG1 unit cell. (b) EBG2 unit cell. (c) Dispersion diagram of EBG1. (d) Dispersion diagram of EBG2.

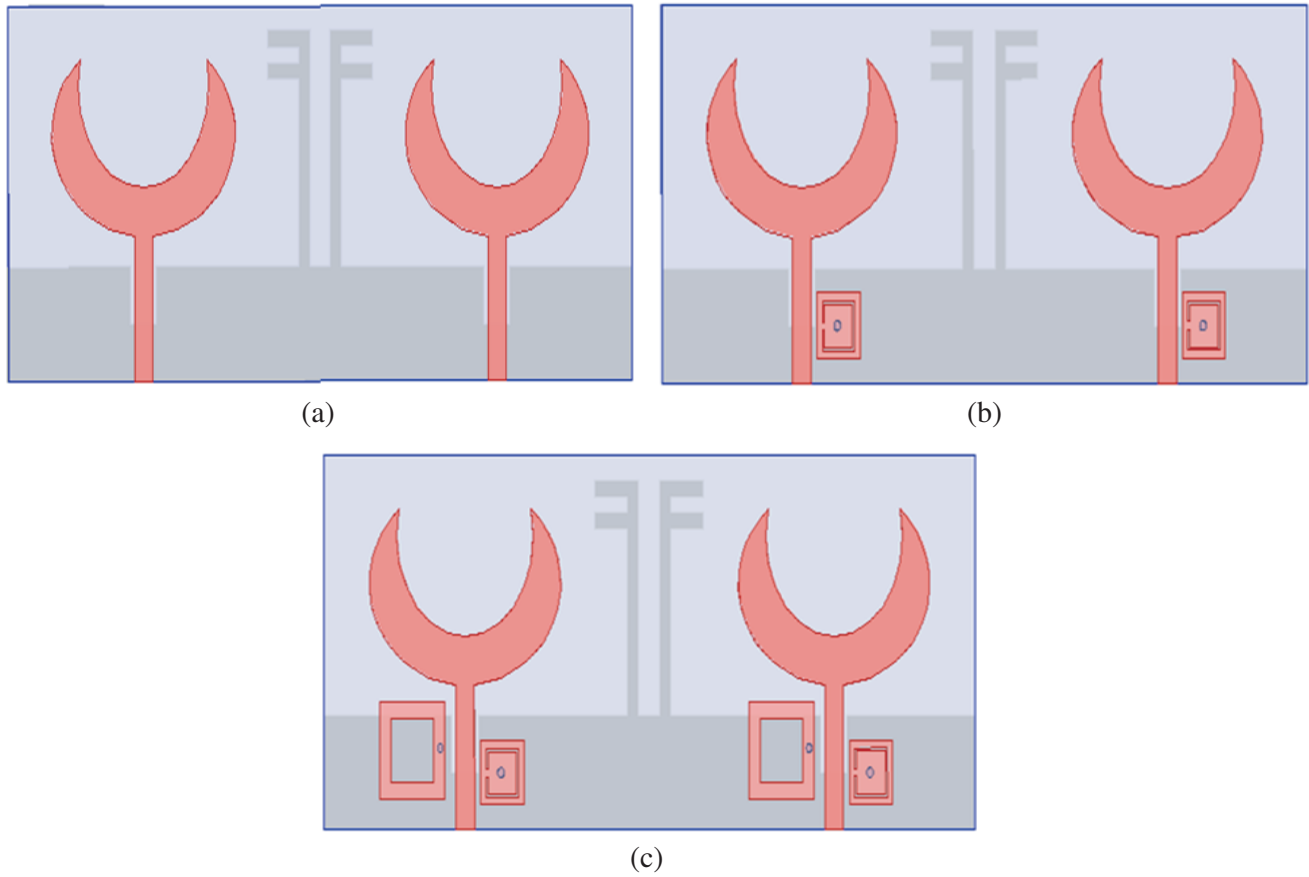


**Figure 5.** Proposed structure with stubs and notches. (a) UWB MIMO antenna with stubs. (b) Single notch-band with stub. (c) Dual notch-band with stubs.

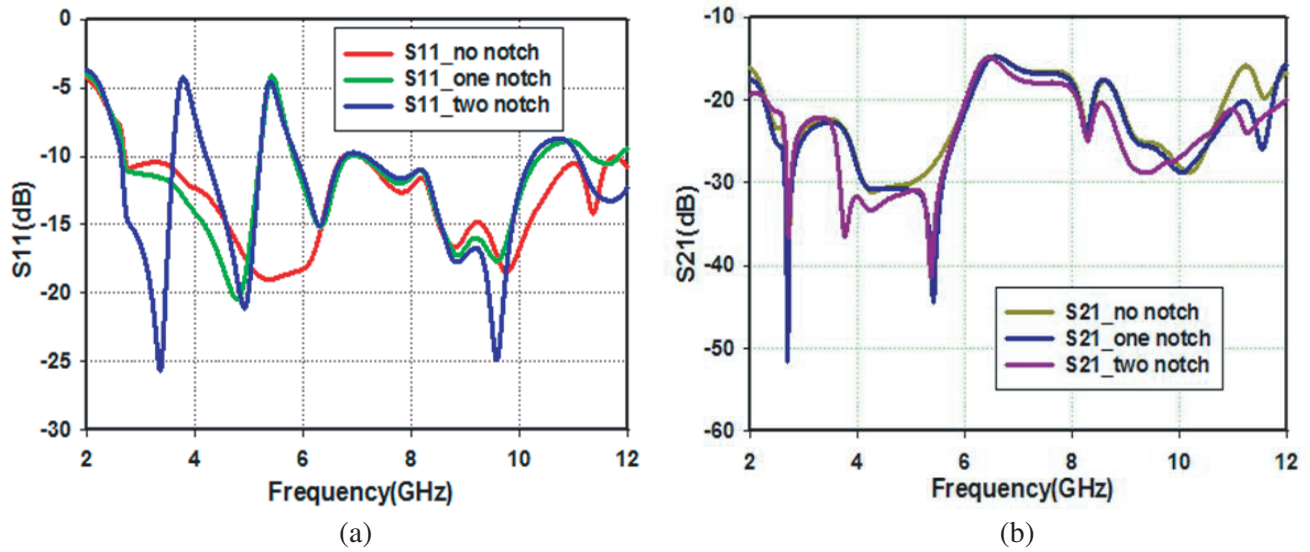


Figure 6. Simulation of the UWB MIMO antenna with stubs and notches. (a)  $S_{11}$ . (b)  $S_{21}$ .

### 3.3. Mutual Coupling of the Proposed Antenna

Figures 7(a) and 7(b) show the loading and unloading of F-pattern stubs over the 2.0–12 GHz frequency band. The simulated  $S_{11}$  and  $S_{21}$  are depicted in Figures 8(a) and 8(b). Mutual coupling ( $S_{21}$ ) is  $< -10$  dB for the absence of decoupling structure. The loading of stubs in the ground will improve the isolation by  $> 15$  dB for the frequency 6–8 GHz and  $> 20$  dB over 2–6 GHz and 8–12 GHz. The antenna’s 10 dB bandwidth ( $S_{11} < -10$  dB) is 2.65–11.65 GHz for  $VSWR < 2.13$  except for the dual-notch band achieved.

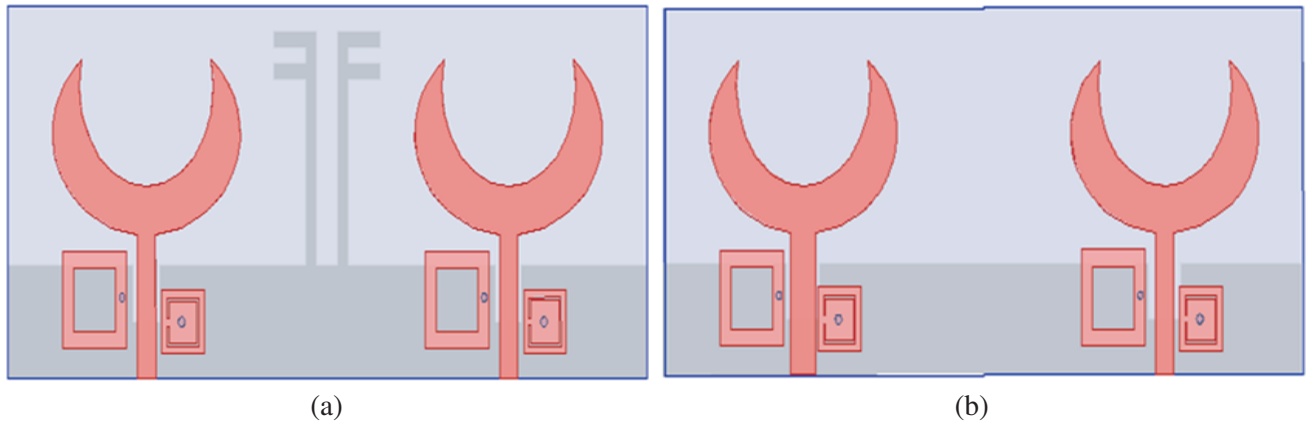


Figure 7. Proposed antenna, (a) with stubs, (b) without stubs.

### 3.4. Surface Current Distribution

The surface current distribution of the proposed antenna in the presence and absence of stubs is studied as mutual coupling between antenna elements as represented in Figure 9. Port terminal 1 (PT1) of the proposed antenna is excited while port terminal 2 (PT2) is terminated with a matching load. Initially, an antenna without a stub is simulated, and the results are plotted in 9(a). It is found that a surface current of large value is induced in the ground and at the notches of antenna 2. The current collected area is represented by the red portion as depicted in the figure, and therefore isolation is less than 15 dB.

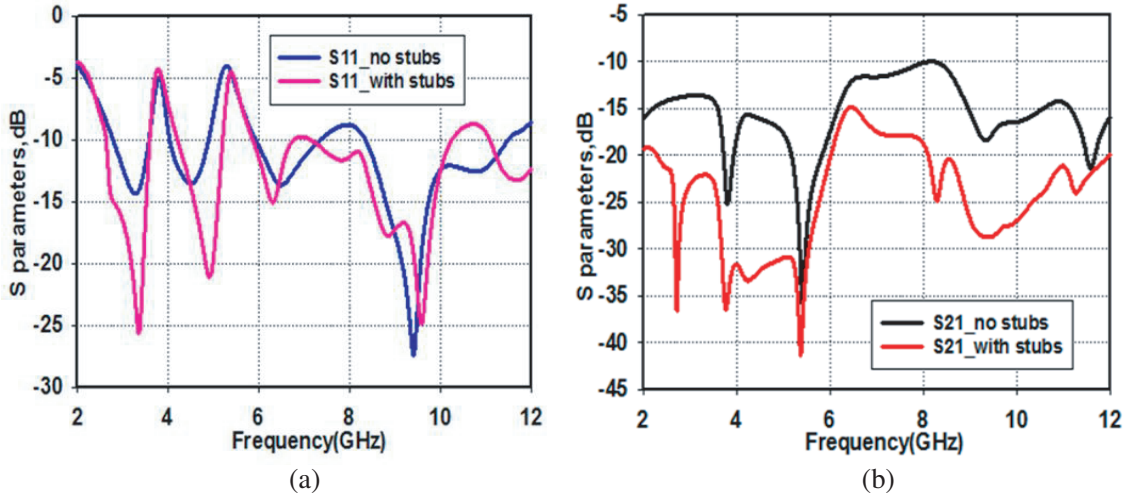


Figure 8.  $S$  parameters, (a)  $S_{11}$ , (b)  $S_{21}$ .

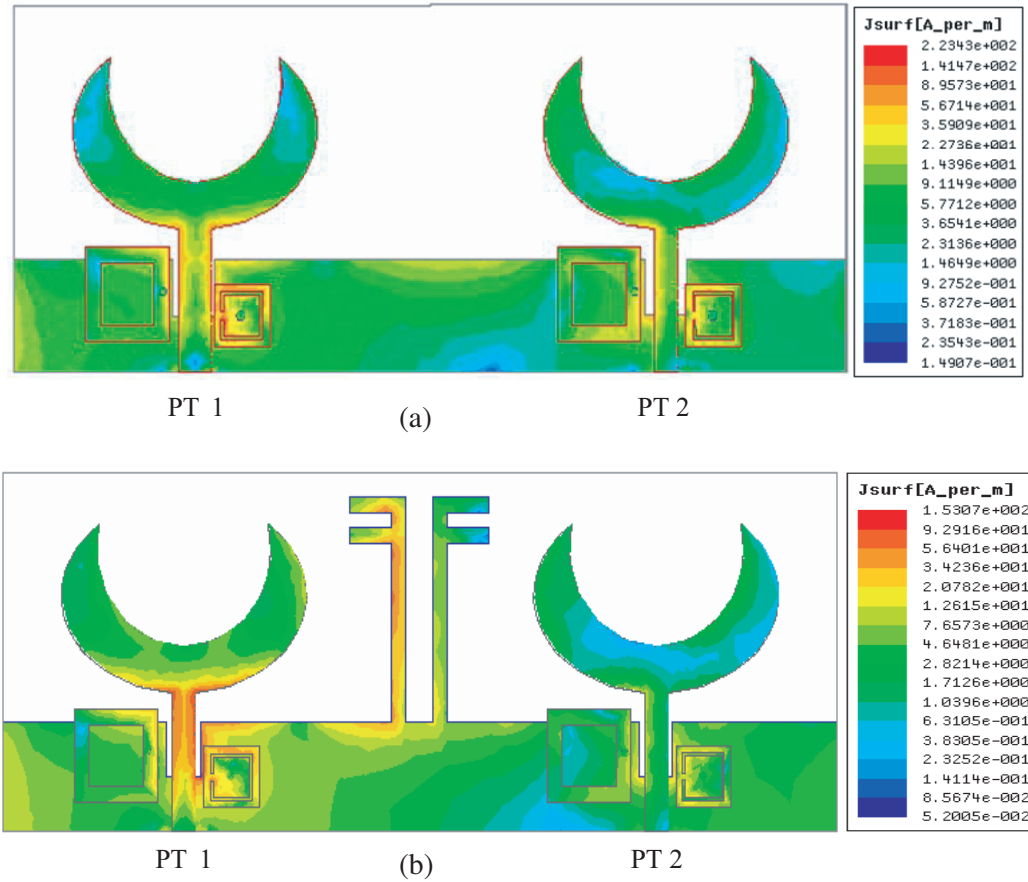
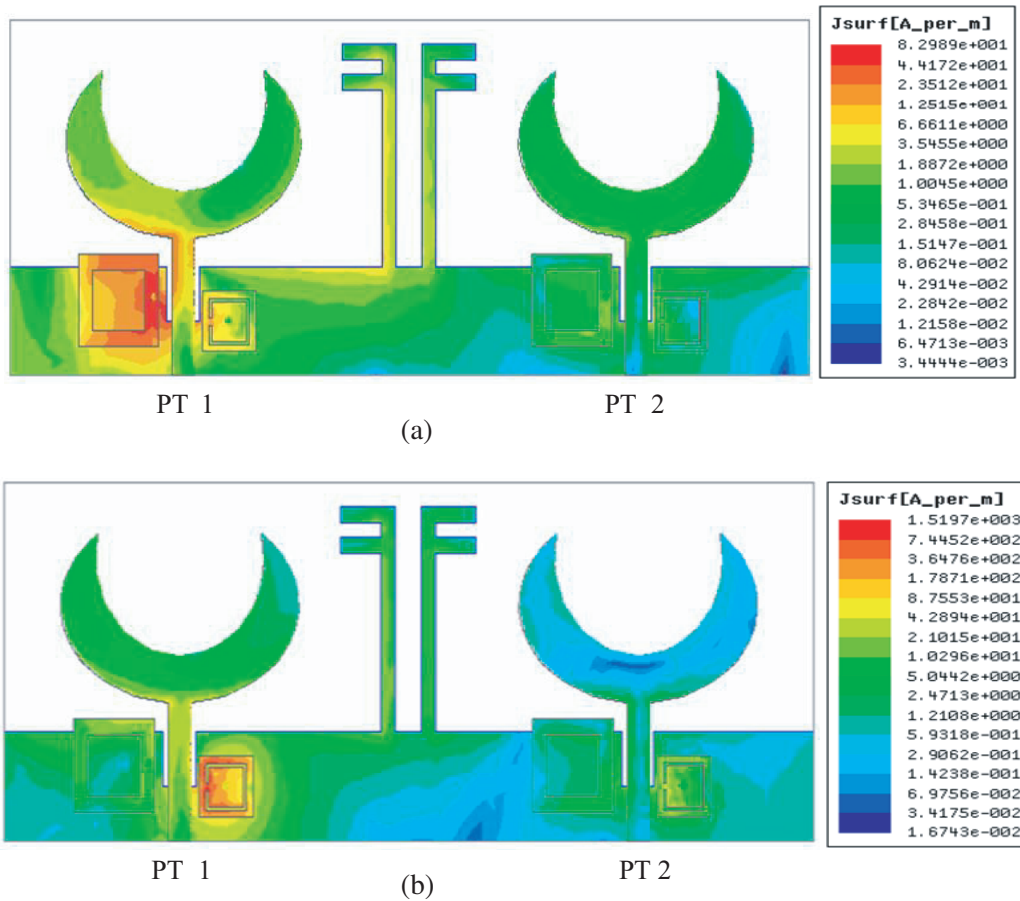


Figure 9. Surface current distribution. (a) Absence of stubs. (b) Presence of stubs.

F-shaped stubs are loaded between antenna elements to improve the isolation. The mutual induction currents of antenna 2 are developed by antenna 1 and F-shaped stubs. If the phases of two induction currents are in opposite directions, then these currents cancel each other, and port isolation is improved by greater than 15 dB as represented in Figure 9(b).



**Figure 10.** Surface current distribution at (a) 3.8 GHz, (b) 5.5 GHz.

Figures 10(a) and 10(b) show the surface current distribution at notch frequencies 3.8 GHz and 5.5 GHz of the proposed antenna. A huge amount of energy is stored on the respective notch which cannot be radiated into the free space at a given notch frequency. Therefore, the frequency bands 3.6–4.2 GHz and 5.15–5.85 GHz are notched at WiMAX and WLAN. The stored energy is shown in the red portion as depicted in the figure.

## 4. RESULTS AND DISCUSSION

### 4.1. Fabrication and Measurements of the Antenna

The designed antenna structure is fabricated on a substrate of FR4 material. The antenna is tested using a full two-port Microwave Vector Network Analyzer N9928A of 26.5 GHz. Figure 11 represents the patch and ground views of the fabricated antenna.

### 4.2. Validation of the Fabricated Antenna

The simulated and measured  $S$  parameters such as  $S_{11}$  and  $S_{21}$  are compared as depicted in Figure 12. The measured working bandwidth ( $S_{11} < -10$  dB) of 2.67–11.62 GHz is achieved with band notch frequency at 3.62–4.18 GHz and 5.17–5.85 GHz corresponding to Wi-MAX and WLAN. The isolation between antenna elements ( $S_{21}$ )  $> 15$  dB over the operating spectrum of the designed antenna. The measured results have small deviation from the simulated due to a copper, connector, and fabrication loss.

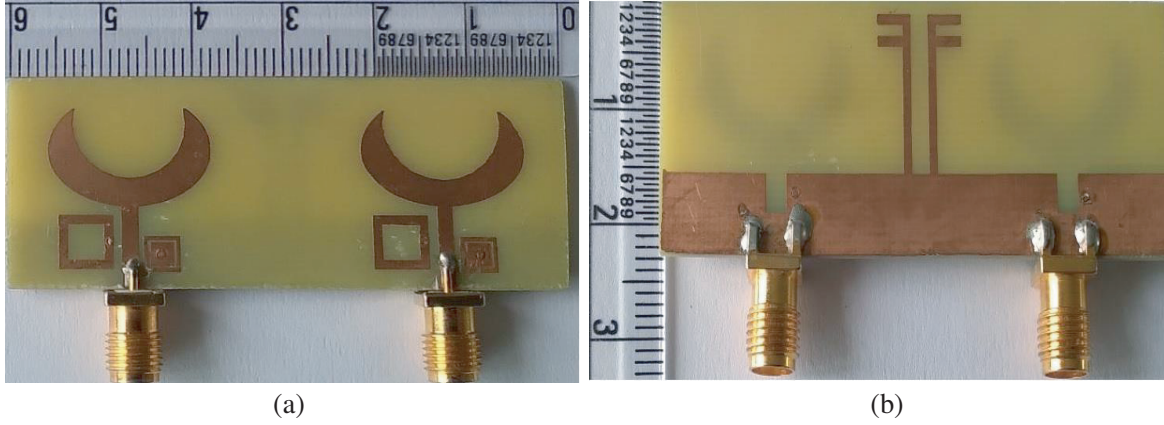


**Figure 11.** Fabricated antenna. (a) Patch. (b) Ground.

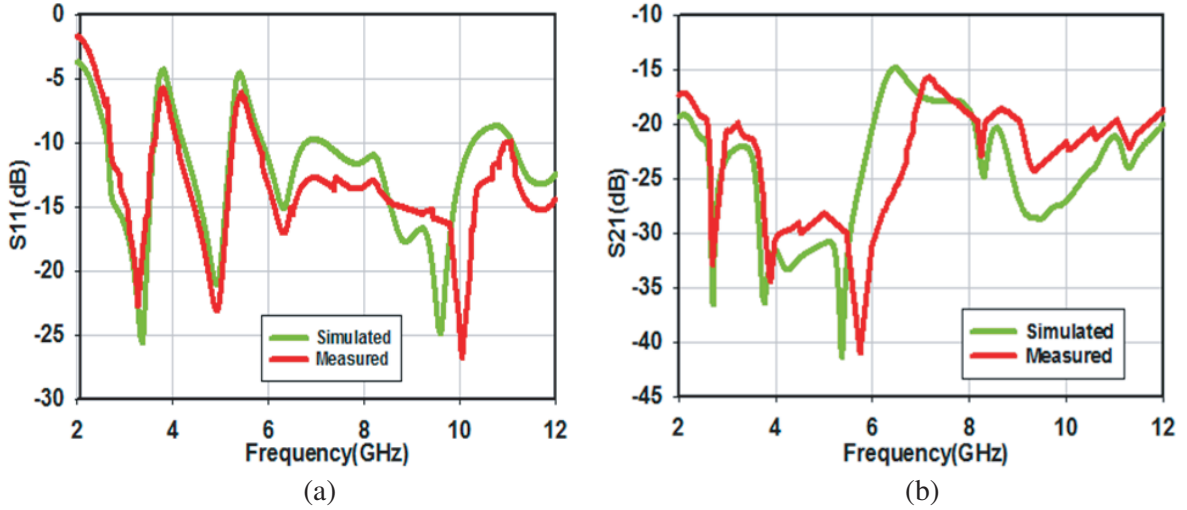


**Figure 12.**  $S$  parameters of the fabricated antenna. (a)  $S_{11}$ . (b)  $S_{21}$ .

### 4.3. Radiation Pattern of the Fabricated Antenna

Figure 13 represents the comparison of simulated and measured radiation patterns of the fabricated antenna in terms of co-polarization and cross-polarization at 4.25 GHz, 6 GHz, and 10.5 GHz in  $H$  and  $E$  planes. The omnidirectional radiation pattern is achieved in the  $H$  plane whereas it is bidirectional in the  $E$  plane. The measured results are in good correlation with the simulated one over the impedance bandwidth of the antenna.

### 4.4. Diversity Performance Parameters

The correlation coefficient evaluates the correlation among multiple-input multiple-output antenna elements and must be  $< 0.5$  to enhance diversity performance.  $S$  parameters of the proposed antenna measure factors of correlation coefficient and are given by Equation (1), where  $\rho_{12}$  is a correlation between antenna 1 and antenna 2. The measured value of Envelope Correlation Coefficient (ECC) is  $< 0.01$  over the entire working bandwidth of the proposed structure. The measured ECC is approximately similar to the simulated results as represented in Figure 14.

$$\rho_{12} = \frac{|S_{11}^* S_{12} + S_{21}^* S_{22}|^2}{(1 - (|S_{11}|^2 + |S_{21}|^2))(1 - (|S_{22}|^2 + |S_{12}|^2))} \quad (1)$$

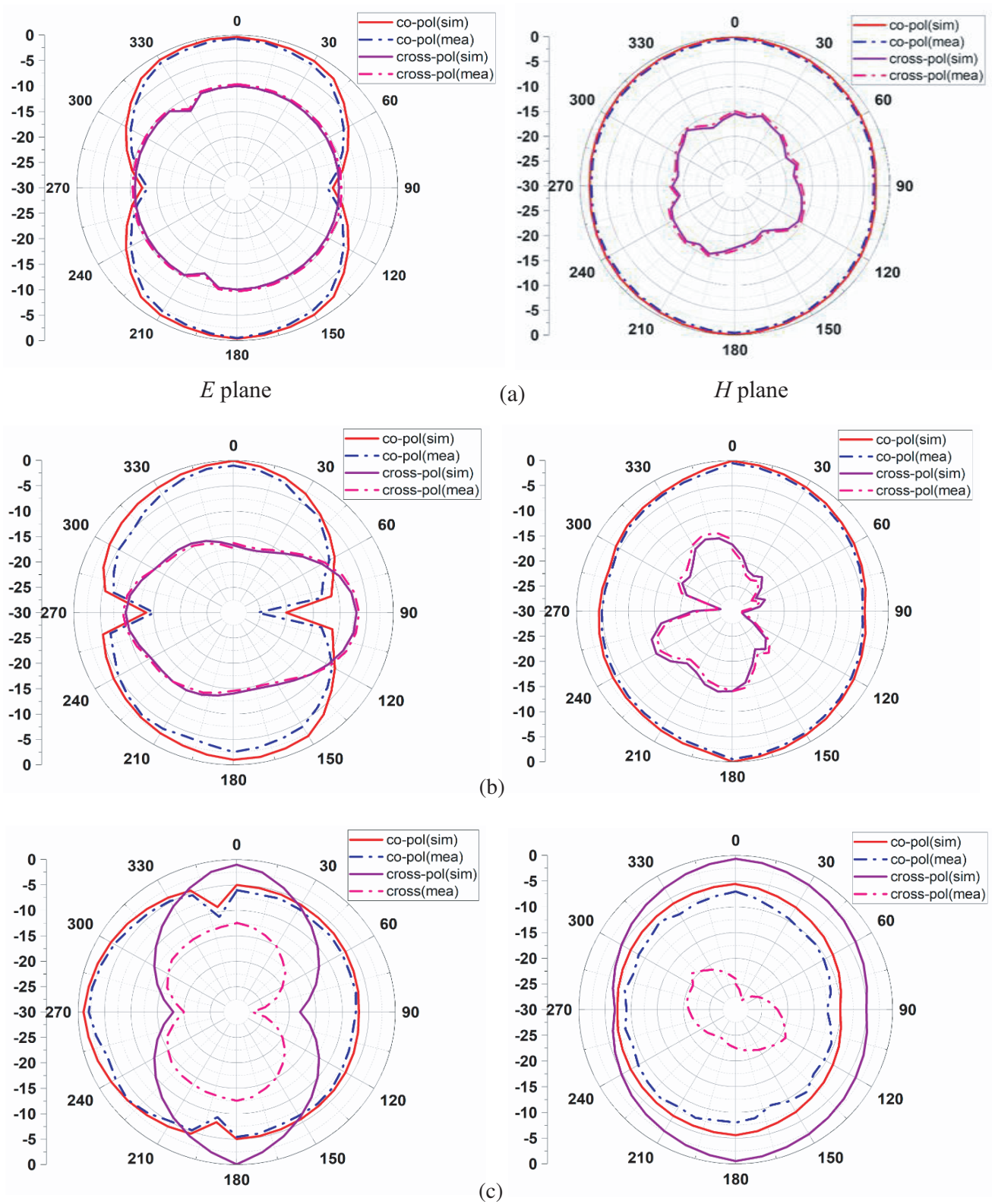


Figure 13. The radiation pattern at (a) 4.25 GHz, (b) 6 GHz, (c) 10.5 GHz.

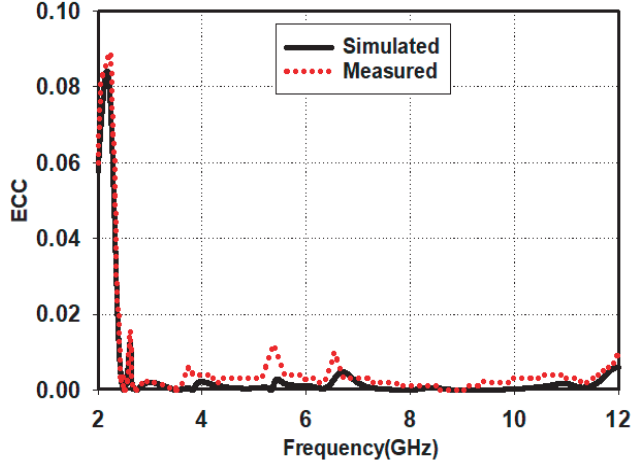


Figure 14. ECC.

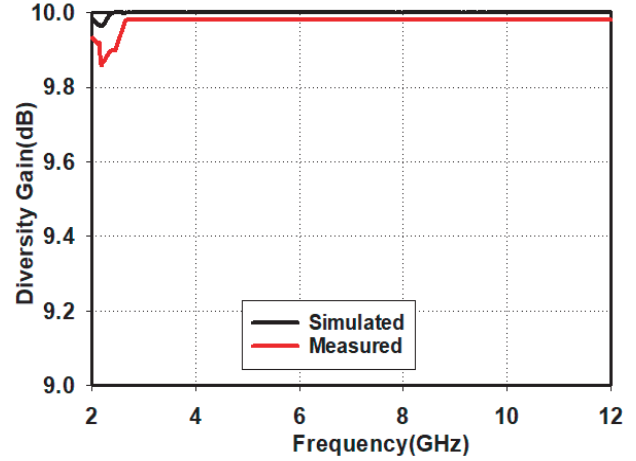


Figure 15. DG.

The performance of diversity gain depends on the correlation coefficient of the MIMO antenna and is given by Equation (2). The measured Diversity Gain (DG) is  $> 9.98$  dB over 2.65–11.65 GHz except for the dual-notch band. The comparative analysis of measured and simulated results is illustrated in Figure 15.

$$DG = 10 * \sqrt{1 - |\rho_{12}|} \tag{2}$$

Total Active Reflection Coefficient (TARC) represents the original feature of  $|S_{11}|$  with a small variation in impedance bandwidth.  $S_{11}$  and TARC are compared as depicted in Figure 16.  $TARC < -10$  dB and measured in terms of  $S$  parameters as given by Equation (3), over the 10 dB BW of the proposed structure.

$$\Gamma_{12} = \sqrt{\frac{(S_{11} + S_{12})^2 + (S_{21} + S_{22})^2}{2}} \tag{3}$$

where  $\Gamma_{12}$  represents the TARC of the proposed antenna.

The number of antennas at the transmitter and receiver will decide the channel capacity of the MIMO antenna. However, correlation among antenna elements also adds some channel capacity loss (CCL) which is measured in bps/Hz and should not be greater than 0.4 bps/Hz. Further, the proposed structure has  $CCL < 0.2$  bps/Hz over the impedance bandwidth ( $S_{11} < -10$  dB) except for the dual rejected bands as depicted in Figure 17.

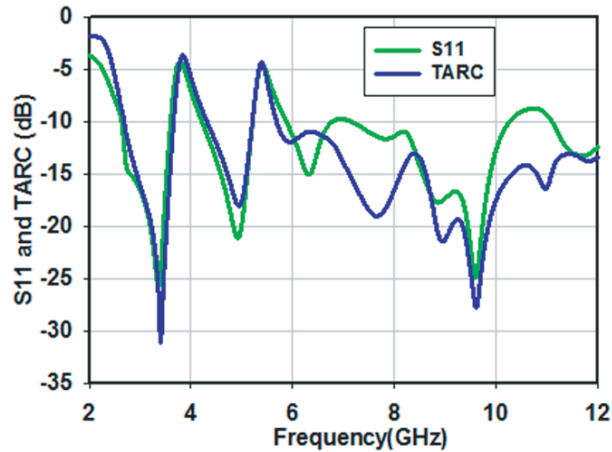


Figure 16.  $S_{11}$  and TARC.

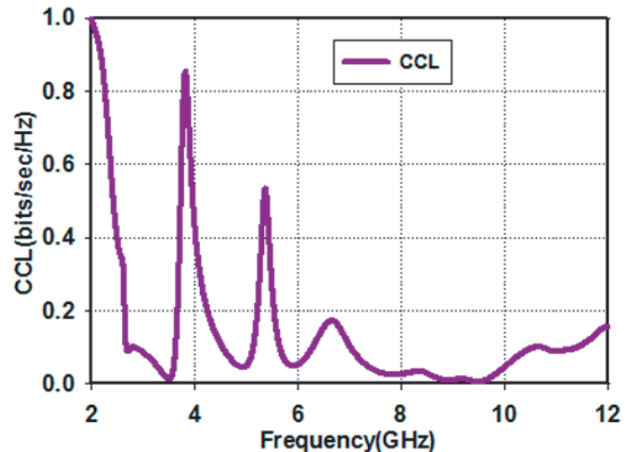


Figure 17. Channel capacity loss (CCL).

### 4.5. Peak Gain

The ability of the proposed structure to transmit and receive signals is measured in terms of peak gain. Figure 18 represents a comparative analysis of measured peak gain and simulated value over the antenna’s operating bandwidth ( $S_{11} < -10$  dB). Peak gain changes from 1 dBi to 7.5 dBi over the available spectrum of 2.65–11.65 GHz except for the dual-notch band. The variation in peak gain is around 6.5 dBi which is acceptable for the proposed structure.

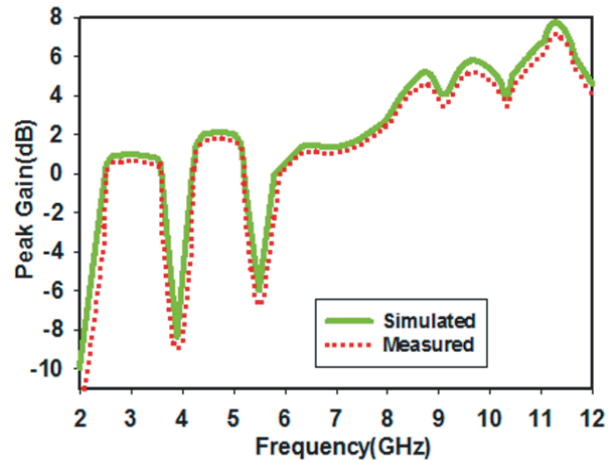


Figure 18. Peak gain.

Table 1. Benchmarking results of the proposed structure with literature.

References	Total ports	Size of an antenna (mm <sup>3</sup> )	Feeding Technique	10 dB BW (GHz)	$S_{21}$ (dB)	Multiband notched (GHz)	ECC	DG	Isolation Techniques
[17]	2	38 × 33.4 × 1.6	Microstrip	2.1–12	> 20		< 0.02	> 9	SRR and slot
[18]	2	50 × 35 × 1	Microstrip	3–11	> 25		< 0.004	> 9	Fence-type structure
[19]	4	50 × 25 × 1.6	Microstrip	2–12	> 17	4.9–6.4	< 0.45	–	Orthogonal /Stubs
[20]	2	46 × 46 × 0.8	CPW	3.1–12	> 17	5.1–5.85	< 0.002	–	Orthogonal Stub
[21]	2	30 × 30 × 0.8	Microstrip	3.6–10.6	> 15	5.15–5.85 7.9–8.4	< 0.03	–	DGS
[22]	2	40 × 40 × 0.8	CPW	3.4–12	> 15	5.15–5.82 7.25–7.75	< 0.05	–	protruded stub
[23]	2	41 × 42 × 0.8	CPW	2.36–12	> 21	3.37–3.98 4.71–5.51	< 0.04	> 9.9	Orthogonal /stubs/DGS
[24]	2	46 × 32 × 1.6	CPW	3–16	> 20	4.95–5.85 7.24–7.87	< 0.025	–	Periodic strips
[25]	4	39 × 39 × 1.6	Microstrip	2.3–13.7	> 22	3.25–3.75 5.08–5.90 7.06–7.95	< 0.02	–	Orthogonal /staircase structure
Work done	2	23 × 60 × 1.53	Microstrip	2.65–11.6	> 15	3.6–4.2 5.15–5.87	< 0.01	> 9.98	Stubs

#### 4.6. Performance Analysis of the Proposed Antenna with the Literature

The comparative analysis of the proposed antenna with research completed on a multiband-notched UWB MIMO antenna in terms of ECC, DG, isolation techniques, 10 dB bandwidth, feeding method, and the multi-notch band is tabulated in Table 1.

### 5. CONCLUSION

The proposed antenna has impedance bandwidth of 2.65–11.65 GHz for VSWR < 2.13, except for the two rejected bands at 3.6–4.2 GHz and 5.15–5.87 GHz corresponding to Wi-MAX and WLAN. The isolation > 15 dB is achieved by loading stubs in the ground over the working spectrum of the proposed structure. Moreover, the proposed antenna has achieved ECC < 0.01, TARC < -10 dB, DG > 9.98 dBi, CCL < 0.2 bps/Hz, and peak gain of 7.5 dB over the ultra-wideband. Therefore, the proposed structure is the ultimate candidate for portable ultra-wideband wireless communication.

### REFERENCES

1. Almalkawiand, M. J. and V. K. Devabhaktuni, "Quad band-notched UWB antenna compatible with WiMAX/INSAT/lower-upper WLAN applications," *Electronics Letters*, Vol. 47, No. 19, 1062–1063, Sept. 2011.
2. Liu, L., S. W. Cheung, and T. I. Yuk, "Compact MIMO antenna for portable devices in UWB applications," *IEEE Transactions on Antennas and Propagation*, Vol. 61, No. 8, 4257–4264, 2013.
3. Le, K., H. Li, X.-H. Wang, and X.-W. Shi, "Miniaturized band-notched UWB MIMO antenna with high isolation," *Microwave and Optical Technology Letters*, Vol. 58, No. 4, 878–881, 2016.
4. Burhan, A., J. Nourinia, C. Ghobadi, M. Majidzadeh, and N. Hatami, "A compact WiMAX band-notched UWB MIMO antenna with high isolation," *Radioengineering*, Vol. 27, No. 4, 2018.
5. Tang, Z., J. Zhan, X. Wu, Z. Xi, L. Chen, and S. Hu, "Design of a compact UWB-MIMO antenna with high isolation and dual band-notched characteristics," *Journal of Electromagnetic Waves and Applications*, Vol. 34, No. 4, 500–513, 2020.
6. Manish, S., "Design and analysis of MIMO antenna with high isolation and dual notched band characteristics for wireless applications," *Wireless Personal Communications*, Vol. 112, No. 3, 1587–1599, 2020.
7. Shah, M. I., I. Ishteyaq, K. Muzaffar, and I. Magray, "A compact band-notched antenna with high isolation for UWB MIMO applications," *International Journal of Microwave and Wireless Technologies*, Vol. 13, No. 6, 634–640, 2021.
8. Tariq, C. H., F. Latif, F. Tahir, M. U. Khan, and X. Yang, "Small-sized UWB MIMO antenna with band rejection capability," *IEEE Access*, Vol. 7, 121816–121824, 2019.
9. Li, Z., C. Yin, and X. Zhu, "Compact UWB MIMO Vivaldi antenna with dual band-notched characteristics," *IEEE Access*, Vol. 7, 38696–38701, 2019.
10. Richa, C., A. K. Gautam, and K. Rambabu, "Tapered fed compact UWB MIMO-diversity antenna with dual band-notched characteristics," *IEEE Transactions on Antennas and Propagation*, Vol. 66, No. 4, 1677–1684, 2018.
11. Yang, Z.-X., H.-C. Yang, J.-S. Hong, and Y. Li, "A miniaturized triple band-notched MIMO antenna for UWB application," *Microwave and Optical Technology Letters*, Vol. 58, No. 3, 642–647, 2016.
12. Pawan, K., S. Urooj, and F. Alrowais, "Design and implementation of quad-port MIMO antenna with dual-band elimination characteristics for ultra-wideband applications," *Applied Sciences*, Vol. 10, No. 5, 1715, 2020.
13. Kumar, R. D., B. K. Kanaujia, and S. Kumar, "Compact four-port MIMO antenna on the slotted-edge substrate with dual-band rejection characteristics," *International Journal of RF and Microwave Computer-Aided Engineering*, Vol. 29, No. 7, e21756, 2019.

14. Salah, S. K. and H. H. Abdullah, "Planar UWB MIMO-diversity antenna with dual notch characteristics," *Progress In Electromagnetics Research C*, Vol. 93, 119–129, 2019.
15. Preeti, P. and D. K. Sharma, "A low-profile quad-port UWB MIMO antenna using a defected ground structure with dual notch-band behavior," *International Journal of RF and Microwave Computer-Aided Engineering*, Vol. 30, No. 9, e22288, 2020.
16. Negin, P., J. Nourinia, C. Ghobadi, and K. Pedram, "A UWB metamaterial-based circularly polarized MIMO antenna with high isolation," *2018 9th International Symposium on Telecommunications (IST)*, 178–182, IEEE, 2018.
17. Pratima, N., A. Nandgaonkar, S. Nalbalwar, and R. K. Gupta, "A compact MIMO antenna with improved isolation for 3G, 4G, WI-FI, Bluetooth and UWB applications," *Progress In Electromagnetics Research C*, Vol. 76, 87–98, 2017.
18. Wang, L., Z. Du, H. Yang, R. Ma, Y. Zhao, X. Cui, and X. Xi, "Compact UWB MIMO antenna with high isolation using fence-type decoupling structure," *IEEE Antennas and Wireless Propagation Letters*, Vol. 18, No. 8, 1641–1645, 2019.
19. Muhammad, K., S. Naqvi, A. Iftikhar, S. Asif, A. Fida, and R. Shubair, "A WLAN band-notched compact four-element UWB MIMO antenna," *International Journal of RF and Microwave Computer-Aided Engineering*, Vol. 30, No. 9e22282, 2020.
20. Paramita, D., A. Karmakar, A. Saha, and S. Huda, "UWB MIMO slot antenna with Minkowski fractal shaped isolators for isolation enhancement," *Progress In Electromagnetics Research M*, Vol 75, 69–78, 2018.
21. Zhu, J., B. Feng, B. Peng, L. Deng, and S. Li, "A dual notched band MIMO slot antenna system with Y-shaped defected ground structure for UWB applications," *Microwave and Optical Technology Letters*, Vol. 58, No. 3, 626–630, 2016.
22. Zhu, J., B. Feng, B. Peng, S. Li, and L. Deng, "Compact CPW UWB diversity slot antenna with dual band-notched characteristics," *Microwave and Optical Technology Letters*, Vol. 58, No. 4, 989–994, 2016.
23. Zhou, J.-Y., Y. Wang, J.-M. Xu, and C. Du, "A CPW-fed UWB-MIMO antenna with high isolation and dual band-notched characteristic," *Progress In Electromagnetics Research M*, Vol. 102, 27–37, 2021.
24. Zhang, J., L. Wang, and W. Zhang, "A novel dual band-notched CPW-fed UWB MIMO antenna with mutual coupling reduction characteristics," *Progress In Electromagnetics Research Letters*, Vol. 90, 21–28, 2020.
25. Tang, Z., X. Wu, J. Zhan, S. Hu, Z. Xi, and Y. Liu, "Compact UWB-MIMO antenna with high isolation and triple band-notched characteristics," *IEEE Access*, Vol. 7, 19856–19865, 2019.
26. Singh, B. S., J. S. Sivia, N. Sharma, and V. Sharma, "Electromagnetic bandgap structure and split ring slot-based monopole antenna for ultra-wideband applications with dual-band notch characteristics," *Engineering Reports*, Vol. 2, No. 10, e12239, 2020.
27. Naveen, J., B. K. Kanaujia, S. D. Gupta, and S. Srivastava, "Dual band-notched EBG structure-based UWB MIMO/diversity antenna with reduced wideband electromagnetic coupling," *Frequenz*, Vol. 71, No. 11–12, 555–565, 2017.